High efficiency excitation of plasmonic waveguides with vertically integrated resonant bowtie apertures

Edward C. Kinzel, Xianfan Xu*

School of Mechanical Engineering and Birck Nanotechnology Center, Purdue University, West Lafayette, IN 47907, USA

*xxu@ecn.purdue.edu

Abstract: In recent years, many nanophotonic devices have been developed. Much attention has been given to the waveguides carrying surface plasmon polariton modes with subwavelength confinement and long propagation length. However, coupling far field light into a nano structure is a significant challenge. In this work, we present an architecture that enables high efficiency excitation of nanoscale waveguides in the direction normal to the waveguide. Our approach employs a bowtie aperture to provide both field confinement and high transmission efficiency. More than six times the power incident on the open area of the bowtie aperture can be coupled into the waveguide. The intensity in the waveguide can be more than twenty times higher than that of the incident light, with mode localization better than $\lambda^2/250$. The vertical excitation of waveguide allows easy integration. The bowtie aperture/waveguide architecture presented in this work will open up numerous possibilities for the development of nanoscale optical systems for applications ranging from localized chemical sensing to compact communication devices.

©2009 Optical Society of America

OCIS codes: (240.6680) Surface Plasmons; (230.7390) Waveguides planar; (130.2790) Guided waves.

References and links

1. R. Kirchain, and L. Kimerling, "A roadmap for nanophotonics," Nat. Photonics **1**(6), 303–305 (2007).
2. E. Ozbay, "Plasmonics: merging photonics and electronics at nanoscale dimensions," Science **311**(5758), 189–193 (2006).
3. W. L. Barnes, A. Dereux, and T. W. Ebbesen, "Surface plasmon subwavelength optics," Nature **424**(6950), 824–830 (2003).
4. S. I. Bozhevolnyi, V. S. Volkov, E. Devaux, J. Y. Laluet, and T. W. Ebbesen, "Channel plasmon subwavelength waveguide components including interferometers and ring resonators," Nature **440**(7083), 508–511 (2006).
5. H. Raether, Surface Plasmons on Smooth and Rough Surfaces and on Gratings, (Springer-Verlag, 1988).
6. J. A. Dionne, L. A. Sweatlock, and H. A. Atwater, "Plasmon slot waveguides: Towards chip-scale propagation with subwavelength-scale localization," Phys. Rev. B **73**(3), 035407–035415 (2006).
7. R. F. Oulton, V. J. Sorger, D. A. Genov, D. F. P. Pile, and X. Zhang, "A hybrid plasmonic waveguide for subwavelength confinement and long-range propagation," Nat. Photonics **2**(8), 496–500 (2008).
8. S. Ramo, J. R. Whinnery, and T. Van Duzer, Fields and Waves in Communication Electronics, (Wiley, 1994).
9. D. M. Pozar, Microwave Engineering, (Wiley, 2003).
10. T. A. Mandviwala, B. A. Lail, and G. D. Boreman, "Characterization of microstrip transmission lines at IR frequencies – modeling, fabrication and measurements," Microw. Opt. Technol. Lett. **50**(5), 1232–1237 (2008).
11. A. Hosseini, H. Nejati, and Y. Massoud, "Design of a maximally flat optical low pass filter using plasmonic nanostrip waveguides," Opt. Express **15**(23), 15280–15286 (2007), http://www.opticsinfobase.org/oe/abstract.cfm?id=144685.
12. S. A. Maier, "Waveguiding: The best of both worlds," Nat. Photonics **2**(8), 460–461 (2008).

13. H. Ditlbacher, J. R. Krenn, N. Felidj, B. Lamprecht, G. Schider, M. Salerno, A. Leitner, and F. R. Aussenegg, "Fluorescence imaging of surface plasmon fields," Appl. Phys. Lett. **80**(3), 404–406 (2002).
14. J. Helszajn, Ridge waveguides and passive microwave components, (Institution of Electrical Engineers, 2000).
15. R. D. Grober, R. J. Schoelkopf, and D. E. Prober, "Optical antenna: towards a unity efficiency near-field optical probe," Appl. Phys. Lett. **70**(11), 1354–1356 (1997).
16. X. Shi, and L. Hesselink, "Mechanisms for Enhancing Power Throughput from Planar Nano-Apertures for Near-Field Optical Data Storage," Jpn. J. Appl. Phys. **41**(Part 1, No. 3B), 1632–1635 (2002).
17. E. X. Jin, and X. Xu, "Finite-Difference Time-Domain Studies on Optical Transmission through Planar Nano-Apertures in a Metal Film," Jpn. J. Appl. Phys. **43**(1), 407–417 (2004).
18. E. X. Jin, and X. Xu, "Obtaining super resolution light spot using surface plasmon assisted sharp ridge nanoaperture," Appl. Phys. Lett. **86**(11), 111106–111108 (2005).
19. E. X. Jin, and X. Xu, "Enhanced optical near field from a bowtie aperture," Appl. Phys. Lett. **88**(15), 153110–153112 (2006).
20. K. Şendur, W. Challener, and C. Peng, "Ridge waveguide as a near field aperture for high density data storage," J. Appl. Phys. **96**(5), 2743–2752 (2004).
21. L. Wang, S. M. V. Uppuluri, E. X. Jin, and X. Xu, "Nanolithography using high transmission nanoscale bowtie apertures," Nano Lett. **6**(3), 361–364 (2006).
22. N. Murphy-DuBay, L. Wang, E. C. Kinzel, S. M. V. Uppuluri, and X. Xu, "Nanopatterning using NSOM probes integrated with high transmission nanoscale bowtie aperture," Opt. Express **16**(4), 2584–2589 (2008), http://www.opticsinfobase.org/abstract.cfm?URI=oe-16-4-2584.
23. L. Wang, and X. Xu, "L.; X. Xu, "High transmission nanoscale bowtie-shaped aperture probe for near-field optical imaging," Appl. Phys. Lett. **90**(26), 261105 (2007).
24. P. B. Johnson, and R. W. Christy, "Optical constants of the noble metals," Phys. Rev. B **6**(12), 4370–4379 (1972).
25. I. H. Malitson, "Interspecimen comparison of the refractive index of fused silica," J. Opt. Soc. Am. **55**(10), 1205–1209 (1965), http://www.opticsinfobase.org/abstract.cfm?uri=josa-55-10-1205.
26. A. Degiron, and D. R. Smith, "Numerical simulations of long-range plasmons," Opt. Express **14**(4), 1611–1625 (2006), http://www.opticsinfobase.org/abstract.cfm?URI=OE-14-4-1611.

1. Introduction

There is a continuous demand to increase the bandwidth/speed while simultaneously reducing the size of electronic, opto-electronic, and sensing devices. Integrated circuits are quickly approaching the bandwidth limit imposed by RC delays in conventional interconnects [1], which limit the microprocessor clock speed despite the continuing reduction in the size of transistors [2]. Conventional photonic components such as optical fibers are attractive because they have sufficiently high bandwidth and low propagation losses. However, optical fibers are fundamentally diffraction limited. In addition, bending light at radii on the order of the wavelength introduces significant losses, further limiting the size of fiber-based devices. Subwavelength confinement is necessary for dense integration in future optical devices including integration with electronic and chemical components.

Recently, a number of nanoscale optical elements have been proposed that utilize surface plasmon polaritons (SPP) to convey and manipulate signals [2,3]. In addition to waveguides and couplers, plasmonic switches and resonators have also been developed [2,4]. SPPs are electromagnetic waves bound to the interface between dielectrics and metal [5]. They have good confinement in the direction normal to the interface and relatively long propagation distances when the width of the waveguide is much greater than the wavelength. Waveguides with hybrid SPP and conventional waveguide modes are also possible [6]. On the other hand, one consideration is that at optical frequencies, metals are significantly lossier and the skin depths become significant relative to wavelength, and as the size of the waveguide shrinks, the portion of the power carried in the metal rather than the dielectric rises. Therefore, there is a tradeoff between mode confinement and propagation distance. Recently, Oulton *et al.* proposed a combination of dielectric and SPP waveguides that have both subwavelength confinement and long propagation lengths [7]. Conventional waveguide geometries developed for the microwave regime, such as microstrip transmission lines [8,9] also support hybrid SPP

like modes at optical wavelengths. Nanostrip waveguides with geometry similar to conventional microwave microstrip transmission lines have been demonstrated at $\lambda = 10.6$ μm [10] and have been proposed for use at $\lambda = 1.55$ μm in components such as branch couplers and filters [11].

A significant challenge for the development of subwavelength plasmonic or hybrid devices is to efficiently excite nanoscale waveguides [12], i.e., coupling far field light from a conventional light source to the subwavelength devices. End fire coupling, where the field distribution of the propagating mode in the waveguide matches that of the incident field, is generally not efficient because of the disparate length scales involved. For SPP waveguides, the momentum mismatch between the SPP mode and a free-space photon of the same frequency must be overcome to achieve coupling from freely propagating light [5]. The two most widely used methods for enhancing the momentum of the incident light through frustrated total internal reflection and using periodic grating require a relatively large launch area which reduces the excitation efficiency. Other experimentally demonstrated methods for launching SPP waves such as via scattering from subwavelength protrusions [13] appear to lack the combination of confinement and efficiency for exciting densely packed arrays of waveguides. In this letter, we report an architecture for locally exciting nanoscale plasmonic waveguides with the use of nanoscale bowtie apertures. Our approach achieves a high coupling efficiency between optical far field and plasmonic waveguide.

2. High efficiency coupling between far field optical source and plasmonic waveguide

Figure 1 shows a schematic of the geometry for coupling between optical far filed and plasmonic waveguide, which consists of four major parts: a metal signal line, a dielectric spacer layer, a metal film into which the bowtie aperture is fabricated, and a transparent substrate. The metal layer that the bowtie aperture is defined in serves as the ground plane for the waveguide. (The combined nanoscale metal signal line and the ground plane resemble the geometry of a microstrip waveguide with reduced dimensions, and can be called nanostrip waveguide.) Light linearly polarized in the y-direction propagating along the $+z$ axis will be captured by the bowtie aperture and effectively focused to the gap region defined by s and d.
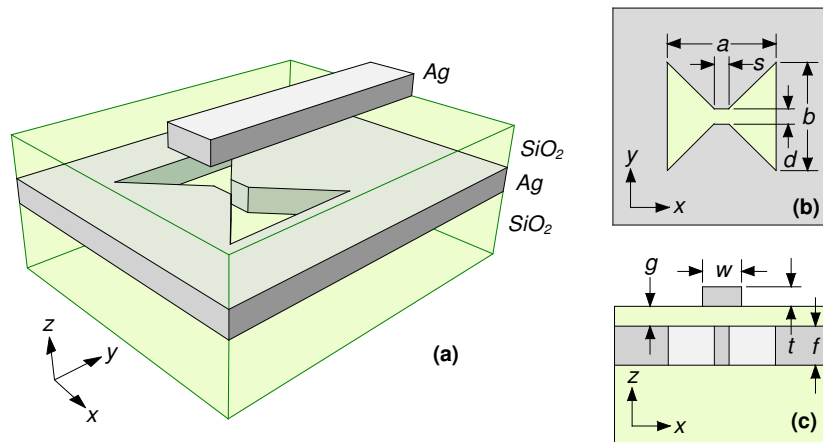

Fig. 1. Bowtie aperture vertically coupled to a waveguide. (a) Three-dimensional rendering. The top gray line is the metal signal line. The bowtie aperture is fabricated in a metal layer (gray). (b) Definitions of the dimensions for the bowtie aperture in a metal film of thickness f and characterized by dimensions, a, b, s, and d. (c) Definitions of the dimensions of the nanoscale plasmonic waveguide, which has width and thickness, w and t, respectively. The center of the metal signal line is directly above the center of the bowtie aperture but separated by a layer of dielectric with thickness g.

(The reason for using a finite gap width s is due to the consideration of fabrication feasibility.) With the proper selection of dimensions, the field emerging in the dielectric spacer layer will efficiently couple to the plasmonic waveguide.

The principal advantage of this geometry is the ability to locally excite waveguides with high efficiency. This is made possible by the bowtie aperture, which is a type of ridge waveguide [8-9,14]. Ridge waveguide apertures (which can be considered as a short waveguide), including shapes other than the bowtie such as 'C' and 'H' have been studied in both the microwave regime and optical frequencies [15-18]. A key advantage of the bowtie aperture is that the cutoff frequency is much lower than a regularly shaped aperture (i.e. circular) with similar field confinement, which leads to dramatically higher transmission [15-18]. At resonance the bowtie aperture effectively receives radiation over a large area and focuses it to the gap region. This provides a high coupling efficiency with the waveguide. An additional advantage of the coupling shown in Fig. 1 is that the antenna geometry is planner and the coupling direction is vertical to the device plane, therefore multiple bowtie apertures can made in parallel for parallel light coupling, modulation, and signal processing. Field concentration and enhancement in bowtie apertures has been experimentally demonstrated, including Near-Field Scanning Microscopy (NSOM or SNOM) measurements [19]. Bowtie apertures have also been used to provide concentrated light sources for data storage [20] and nanolithography [21-22], and as high efficiency light collectors for high resolution imaging [23].

Figure 2 (Media 1) shows the coupling of the electric field from the bowtie aperture to the waveguide. The telecommunication wavelength, 1.55 μm is used throughout this work, although our approach is generally applicable to optical frequencies. We select silver for the metallic portions of the structure because of its low losses at these wavelengths. Fused silica is used for the dielectric because of its low permittivity which gives a high contrast to silver. The spectral electromagnetic properties for silver (ε_m = -129.1 + 3.283j) and fused silica (ε_d = 2.085) are taken from [24] and [25], respectively. Numerical calculations are obtained using commercial frequency domain finite-element method software (HFSS from Ansoft LLC.), which has been previously used to analyze problems involving SPPs at optical frequencies [20,26]. An adaptive mesh is used, and the mesh density was initially specified in the critical regions (5 nm maximum edge length) and the adaptive mesh refinement process allowed to continue until the energy in the system had converged to less than 1%. A Perfectly Matched Layer (PML) was used to terminate the waveguide and radiation Absorbing Boundary Conditions (ABC) for the other free surfaces. The figure (and Media 1) shows the geometry in Fig. 1 illuminated by a plane wave propagating in the +z direction and linearly polarized with the electric field in the y direction, at the instant when the electric field in the substrate is near its maximum (the metal signal line extends to infinity in both directions). The instantaneous (at a given phase angle) electric field intensity is plotted, and the figure shows the standing wave, generated by the ground plane, along with the wave fronts propagating down the nanostrip. The gap d and s in this calculation and all calculations shown below are chosen to be 25 nm since this dimension can be fabricated in a metal film relatively easily using focus ion beam milling or electron beam lithography. Figure 2 (Media 1) shows that the incident wave with wave vector k_0 couples through the bowtie aperture to the mode propagating in the ±y directions down the waveguide, with wave vectors indicated by $k_{1\pm}$. The ground plane is thick enough that the incident plane wave does not interact with the waves in the waveguide except in the region immediately surrounding the aperture. Figure 2(b) shows the lateral confinement of the light in the metal signal line. Figure 2(c) shows the peak and instantaneous electric fields along the centerline of the strip (y = 50 nm) along with the power carried in the line.
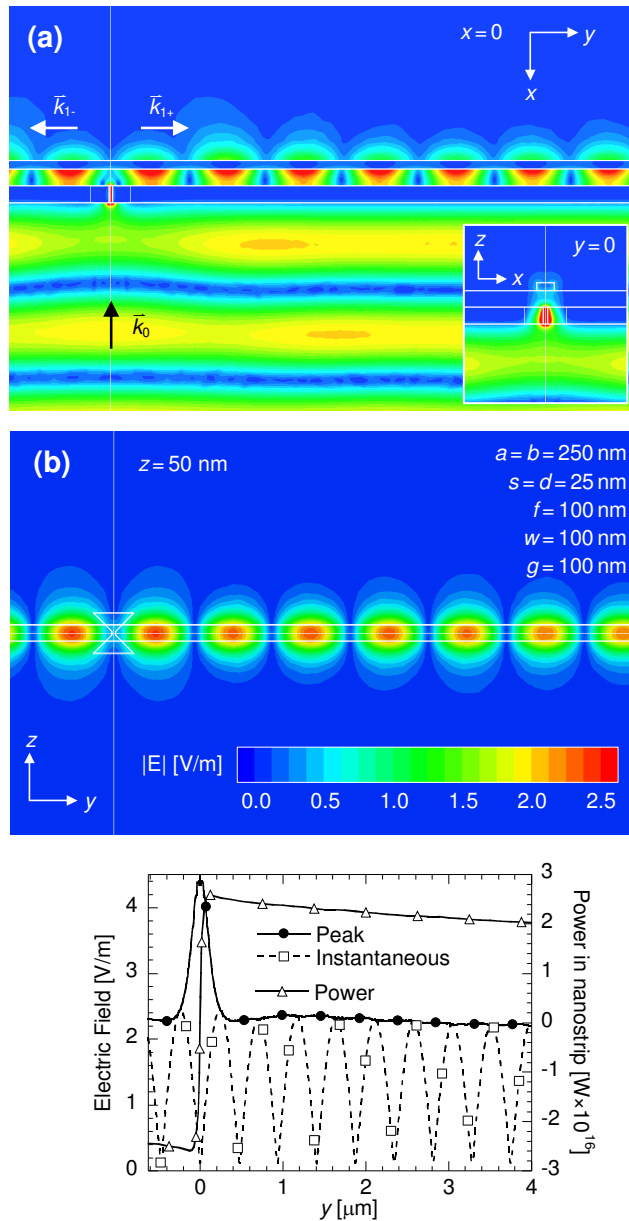
Fig. 2. Instantaneous electric field distribution showing coupling between a plane wave and the waveguide. A y-polarized plane wave incident on a 250 nm bowtie aperture (25 nm gap) coupling to a 100 wide transmission line separated from the bowtie aperture by a gap of 100 nm. The magnitudes of the electric fields are plotted: (a) (Media 1) yz plane through the centre of the aperture with inset showing xz plane. The black arrow of the incident wave vector points to the center of the bowtie aperture. (b) xy plane midway through the dielectric region ($z = 50$ nm). The magnitude of the incident electric field is 1 V/m in the fused silica substrate. In the figures, the field is saturated at 2.5 V/m for clarity. A movie of light propagation from far field into the waveguide is provided in supplementary information. (c) Peak and instantaneous values of the electric field along the centerline of the nanostrip ($z = 50$ nm) and the power carried in the line as a function of distance from the center of the aperture.

In the waveguide, light is attenuated as it propagates along the waveguide due to metal losses. After an initial transition length (less than 0.5 μm from the center of the aperture), the field decays exponentially. The power carried by the waveguide at a given point y can be obtained by integrating the y component of the Poynting vector over the xz plane through that point. The coupling efficiency from a far field light source to the waveguide is computed as the ratio between the equivalent initial power in the waveguide directly above the bowtie aperture and the power incident on the bowtie aperture within a diffraction limited spot at the 1.55 μm wavelength (945.5 nm diameter). This equivalent initial power is obtained by fitting the exponential decay function to the power in the waveguide outside the transition length ($y >$ 0.5 μm) and extrapolating back to $y = 0$. The power in the waveguide is equally divided between the two branches (traveling in the $\pm y$ directions). Figure 3 shows how this coupling efficiency varies with geometry parameters. More than 30% of the power within a diffraction limited spot can be coupled into the waveguides (including power traveling in both directions of the waveguide). It should be noted that techniques such as oil immersion lenses can be used to reduce the diffraction–limited spot size, which will increase the coupling efficiency defined here. On the other hand, if the open area of the bowtie aperture is used to compute the total incident power, the efficiencies shown in Fig. 3 will increase by a factor of 22, making the highest efficiency greater than 660%. That is, a properly dimensioned bowtie aperture couples as much as six times of the radiation on its opening area into the waveguide. It is important to note that these results are only for light polarized in the y-direction. The coupling to the aperture is very sensitive to polarization and if the light is polarized in the x-direction, the coupling to the nanostrip aperture is negligible.
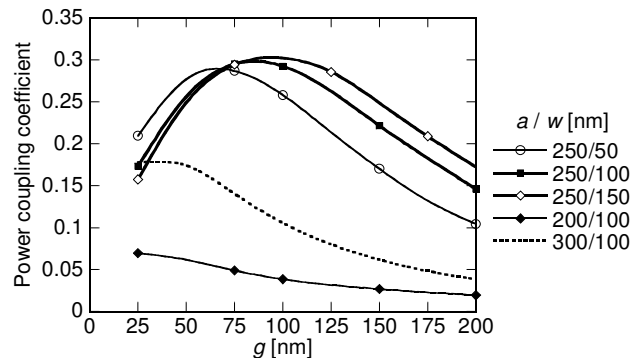

Fig. 3. Coupling efficiency from a far field light source to the waveguide. The far field light source is assumed to be a diffraction limited spot incident on the bowtie aperture with a diameter of 945.5 nm. For the bowtie aperture, $a = b$ is used. $s = d = 25$ nm, $f = 100$ nm, and $t = 50$ nm.

The dependence of the coupling efficiency on the geometric parameters can be seen from Fig. 3. The outline dimensions of the aperture, a and b ($a = b$ is used), dramatically affect the coupling efficiency. This is due to the resonance of the aperture which is to be discussed in more detail later. For the off-resonance apertures ($a = 200$ and 300 nm), increasing the gap decreases the coupling efficiency. For the resonant aperture ($a = 250$ nm), there is an optimum gap g which varies with the width of the waveguide. Other parameters have a lesser effect on the coupling efficiency. In order to obtain a better understanding of how various parameters affect the coupling efficiency, we provide analyses below of the individual components, starting with the light propagation along the waveguide and then the transmission and resonance of the bowtie aperture.

3. Detailed analysis of coupling of EM field between the plasmonic waveguide and the bowtie aperture

The field distribution in the waveguide past the transition region (~ 0.5μm or less) can be obtained from its eigenmode solution [26]. The power and field distributions in the waveguide are plotted in Fig. 4(a). This is a hybrid mode resembling the quasi-TEM field distribution for a conventional microstrip albeit with significant field penetration into the metal films. There are longitudinal electric and magnetic components but their magnitudes are two orders of magnitude lower than those of the transverse components. The figure shows that the field is well confined within the waveguide with the majority of the power carried in the dielectric layer and very high intensities at the corners. The mode area, A_m, is a metric of the field confinement and is defined as the ratio of the total power carried through a cross-section of the waveguide to the peak intensity in the same cross-section:

$$A_m = \frac{\iint_A \mathrm{Re}\left\{\mathbf{E} \times \mathbf{H}^*\right\} dA}{\mathrm{Re}\left\{\mathbf{E} \times \mathbf{H}^*\right\}_{max}} \tag{1}$$
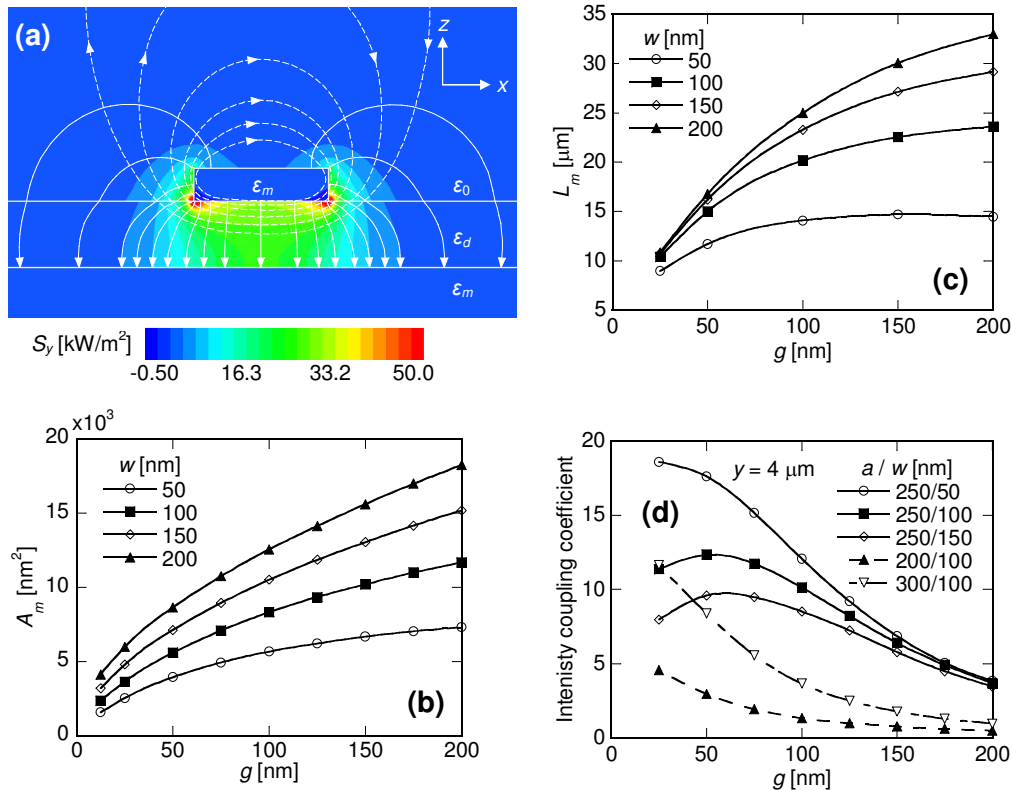

Fig. 4. Properties of the nanostrip waveguide. (a) Magnitude of the Poynting vector along the waveguide with the size of $w = 200$ nm, $g = 100$ nm and $t = 50$ nm. Solid field lines show the direction of the electric field and dashed indicate the direction of the magnetic field. The waveguide is transmitting 1 nW total power. The intensity is saturated at 50 kW/m² for clarity. (b) Mode area, defined as the ratio of the total power carried in the transmission line divided by the peak power intensity. (c) Propagation length for different geometries. (d) Ratio between the peak intensity in the waveguide at 4 μm away from the center ($y = 4$ μm) and the incident intensity.

The sharp corners on the metal signal line lead to a very high field. The maximum intensity used in Eq. (1) is the intensity averaged over a 4 nm diameter circle centered about the corners. This underestimates the peak intensity; however, it allows a finite radius which would result from any practical fabrication method. The mode area vs. waveguide geometry is shown in Fig. 4(b), which shows that a waveguide defined by $w = g = 100$ nm and $t = 50$ nm has a field confinement better than $\lambda^2/250$. Also, it can be seen that the mode area is roughly proportionate to cross sectional area of the waveguide. Figure 4(c) shows how the propagation lengths in the waveguide are affected by the waveguide dimensions, which is defined as the distance at which the power diminishes to 1/e of its original value, and is equal to

$$L_m = 1/2 \operatorname{Im}\{k\} \tag{2}$$

where k is the complex propagation constant. Generally it can be seen that the propagation length is longer for the larger separations and wider metal signal lines. This can be attributed to more of the power being carried in the dielectric as opposed to the metal portions of the waveguide.

The peak field intensities in the waveguide are significantly higher than that of the incident plane wave and are confined along the edges of the metal signal line. The peak intensity (4 μm from the aperture) can be nearly 20 times of that of the incident wave as shown in Fig. 4(d). The tight field confinement and high peak intensity are particularly useful for applications such as molecular sensing.

As mentioned previously, a key advantage of using a bowtie aperture is its ability to generate a subwavelength spot with high transmission, effectively focusing a plane wave to a spot determined by the gap dimensions s and d. This makes it ideally suited for coupling light locally to a nanoscale device. In the absence of the metal signal line or other features near the exit of the bowtie aperture, the light emerging from the bowtie aperture will behave similarly to a Hertzian dipole. A portion of the transmitted energy couples to spherical harmonics and propagates into the far field but most of the energy remains in the evanescent near field. The electric and magnetic field distributions for a bowtie aperture defined in a 100 nm thick silver film on a fused silica substrate (the other side is bound by free space) are shown in Fig. 5. With a given geometry, the transmission is a strong function of the incident light wavelength, and peaks at a certain wavelength due to resonance as shown in Fig.5(c). This explains why the 250 nm bowtie aperture provides the best coupling efficiency with the waveguide shown in Fig. 3.

The analyses of the mode shapes of the nanostrip waveguide and the resonant bowtie aperture provide insight into their interaction when they are combined. Figures 4(a) and 5(a), (b) illustrate the similarity of the field distributions of the two structures. In particular, the magnetic field distribution at the exit of the bowtie aperture as shown by the field lines in Fig. 5(b) (the directions of the field) aligns well with the field surrounding the metal signal line shown in Fig. 4(a). However, when the bowtie aperture and the waveguide are combined, the field distributions around the bowtie aperture are affected by the presence of the nanostrip waveguide and vice versa. This interaction necessitates simulations of the entire structure which is shown in Fig. 6. The electric field emerging from the bowtie aperture quickly becomes directed in the vertical direction in the xy plane and confined below the metal signal line while the magnetic field envelops the metal signal line, providing the necessary components of the propagating wave along the waveguide as shown in Fig. 4(a). Also noted is the lack of magnetic confinement in and near the bowtie aperture, indicating that the magnetic field plays an important role in the coupling. The field intensities and the field lines shown in Fig.6 provide an explanation of the coupling between the bowtie aperture and the waveguide. On the other hand, the complex interaction between the aperture and nanostrip make it difficult to achieve the optimum coupling without numerical computations.
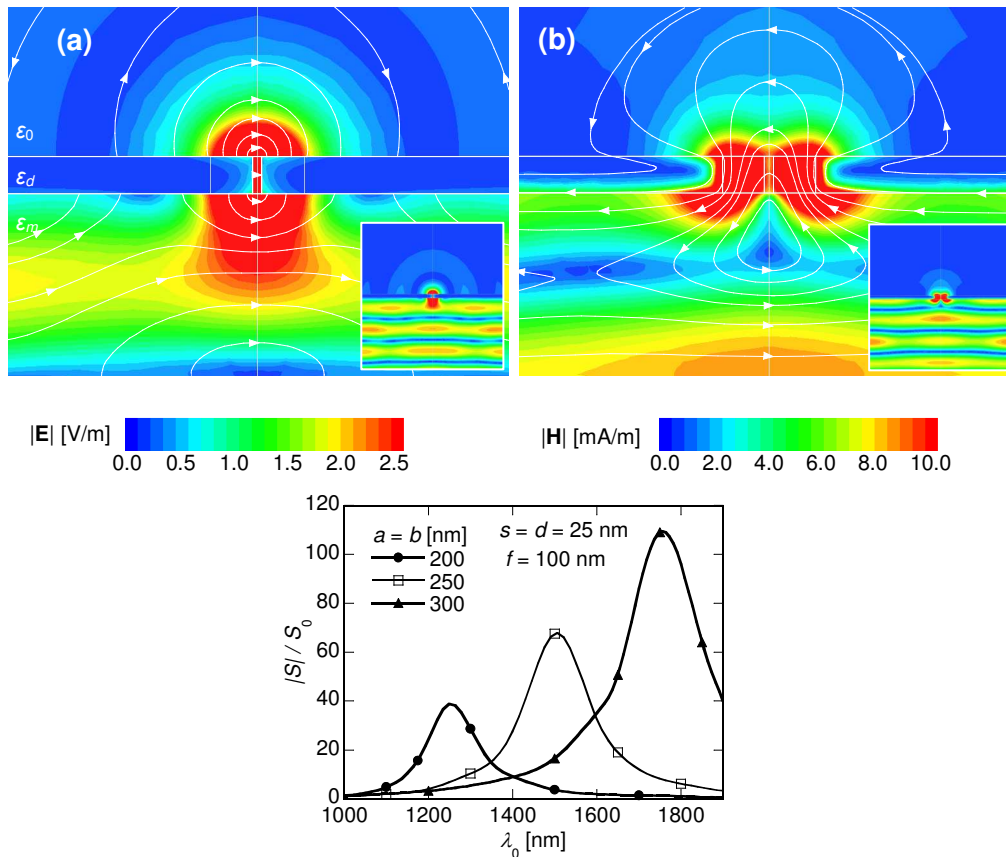
Fig. 5. Transmission through a bowtie aperture. Field distribution for a bowtie aperture ($a = b =$ 250 nm, $s = d = 25$ nm, $t = 100$ nm) in a silver film on a fused silica substrate at one instant in time. (a) The electric field on the yz plane (saturated at 2.5 V/m for clarity). Field lines show the direction of the electric field. (b) The magnetic field on the xz plane (saturated at 10 mA/m for clarity). Field lines show the direction of the magnetic field. (c) The ratio of the intensity at the centre of the gap on the exit plane to the intensity of the incident plane wave for different bowties ($s = d = 25$ nm, $f = 100$ nm) as a function of wavelength, showing strong spectral dependence and resonance.

Once the wave is launched in the waveguide, its propagation characteristics are determined since the response in the waveguide is no longer affected by the choice of bowtie dimensions after the initial transition length. From Figs. 3 and 4, it is seen that there is a tradeoff between the coupling efficiency, the propagation length in the waveguide, and the field confinement. A larger separation between the bowtie and the metal signal line allows a longer propagation length, but the amount of light coupling to the bowtie aperture is less. A wider line width is generally better for both coupling efficiency and longer propagation length, but at the expense of the field confinement. On the other hand, in practice, one can use signal lines with variable widths, i.e., a wider width directly above the bowtie aperture for a higher coupling efficiency, and tapered down to a narrower width at the desired locations. Standard microwave engineering approaches such as impedance matching can be used to guide the energy around corners and couple to other waveguides [8-9, 11]. Alternatively, the signal line can be also used to end-fire couple into other type waveguides that may have longer propagation length, such as the waveguide proposed by Oulton et al. [7], SPP stripe

waveguides (a metal signal line without the ground plane), other optical elements such as switches and sensing elements, or providing sources for pumping in an optical circuit.
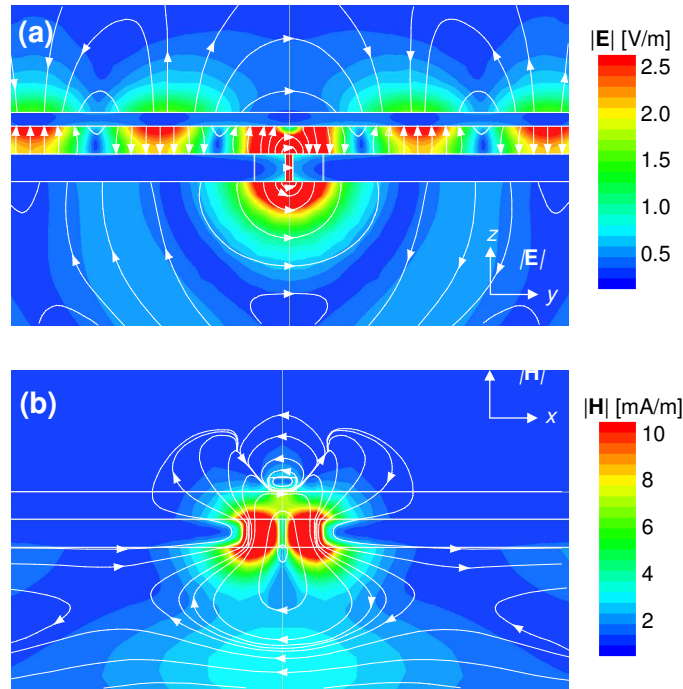

Fig. 6. Interaction between the bowtie aperture and nanostrip waveguide. The geometry parameters are $a = b = 250$ nm, $f = 100$ nm, $s = d = 25$ nm, $w = 100$ nm, $g = 100$ nm, and $t = 50$ nm. (a) Electric field on yz plane and (b) magnetic field on xz plane (both passing through the origin). The field lines and arrows show the directions of the fields.

4. Conclusions

In summary, we described a nanoscale bowtie aperture-based architecture for vertically coupling far field light sources into nanoscale waveguides with high efficiency. The key to this high efficiency is the resonant excitation of the bowtie aperture. With proper design, the localized light spot produced by the bowtie aperture are well matched to the propagating mode in the waveguide. The vertical coupling between the far field light source and the waveguide also facilitates practical implementation. Numerous nanoscale optical devices for applications such as chemical sensing and optical communication can be envisioned based on the bowtie antenna/waveguide architecture.

Acknowledgments